Journal of Civil Engineering, Science and Technology

Volume 17, Issue 1, April 2026, 71-86

ANALYSIS OF COMBINED PILE RAFT UNDER AXIAL LOAD

Shailja Gupta, Vishwas A. Sawant and P.K. Gupta
Civil Engineering Department, IIT Roorkee, Roorkee, 24667 Uttarakhand, India.

Date received: 05/05/2025 Date accepted: 11/03/2026
*Corresponding author's email: vishwas.sawant@ce.iitr.ac.in
DOI: 10.33736/9638.2026

Abstract — A pile raft foundation is recognised as the most efficient foundation for high-rise buildings in comparison to conventional group pile foundations. But usually, in the case of practical designs, the contribution of the raft is ignored, and the foundation is designed as a pile foundation alone. Hence, in the present study, an attempt has been made to determine the Combined Pile Raft Foundation (CPRF) coefficients of pile rafts subjected to vertical load. A further parametric study is performed to investigate the effect of pile length, raft thickness, friction angle, and soil modulus on the response of a pile raft. The CPRF coefficient of the pile increases with its length. Furthermore, the settlement of CPRF decreases with an increase in the pile length. Settlement of CPRF decreases with an increase in friction angle as well as soil modulus. The CPRF coefficient of piles decreases, and that of a raft increases with an increase in friction angles. The CPRF coefficient does not alter much with soil modulus.

2462-1382 / © 2026 The Author(s). Published by UNIMAS Publisher. This is an open access article under the CC BY-NC-SA 4.0 license (http://creativecommons.org/licenses/by-nc-sa/4.0/).

***Keywords*:** pile raft, pile length, raft thickness, CPRF coefficient, settlement

1. INTRODUCTION

These days the availability of space for constructing new buildings has decreased significantly. Hence, instead of constructing new buildings, people started to acquire more vertical space, thereby increasing the demand for high-rise buildings. But with the increase in the building height, the number of piles tends to increase, thereby affecting the price of these buildings. Also, with the use of the foundations in the construction of high-rise buildings, settlement was not controlled effectively. Hence, the designers are looking for an alternative option. By focusing on all the above aspects, a combined pile raft foundation (CPRF) is preferred over a conventional group pile for high-rise buildings. In CPRF, piles act as settlement reducers, which reduces total and differential settlements. Recently, CPRF has been recognised as the most viable and effective foundation due to the utilisation of the ultimate capacity of both pile and raft, thereby resulting in considerable savings with the use of fewer piles without compromising the durability of the foundation system. Amplification and lateral displacement of superstructures were dependent on the system frequency at the lower-level base acceleration [1]. Chanda et al. [4] observed that piled-raft lateral capacity increases due to combined V-M-H loading more than that of independent capacity. Clancy and Randolph [5] performed parametric studies and described the hybrid approach for the analysis of piled raft foundations. Peak responses to structure and soil were greatly reduced with the help of CPRF and thus can be useful for nuclear power plants constructed on soft soil [8]. Horikoshi et al. [11] performed a series of shaketable tests on CPRFs and pile groups by using a geotechnical centrifuge with different connection conditions for piles. Kang et al. [13] investigated the seismic response of CPRFs under clay with flexible and stiff piles using centrifuge tests. The application of CPRF as a foundation for a high-rise building in settlement-sensitive Frankfurt clay has proven to be an effective and economical foundation system, achieving a settlement reduction of more than 50% compared to raft foundations and reducing pile costs by more than 60% compared to conventional pile foundations [14]. Matsumoto et al. [16] investigated the effect of the height of the horizontal loading point as well as the connection condition of piles under horizontal load at 1-g gravitational field. When the input frequency was lower than the resonant frequency, the behaviour of stacked rafts during shaking was like piled rafts subjected to static horizontal loading [17]. Matsumoto et al. [18] investigated the behaviour of piled rafts, pile groups, and rafts alone subjected to static vertical and cyclic horizontal tests with different pile head connections at 1-g centrifugal tests. Concentrated pile arrangement reduces the bending moment and restricts the maximum bending moment of the raft [19]. As pile length increases, the natural radial frequency of CPRFs decreases [20]. In comparison to slab foundation settlement, CPRF was much smaller [21]. However, the effect of nonlinear soil behaviour is more critical at smaller pile spacings [22]. Ta and Small [23] presented a method of analysis for piled rafts based on the interactions of the raft, pile and soil. Yamashita et al. [25] reported that at the end of the observation period, the

measured settlements of all the buildings were 19 to 24 mm, and the ratios of the load carried by the piles to the effective load were 0.61 to 0.93. Yamashita et al. [26] investigated the static and seismic behaviour of CPRFs with grid-form deep cement mixing walls supporting a 12-storey base-isolated building in Tokyo. Yamashita et al. [25] reported that before the earthquake, the load-sharing ratio of piles was 0.72, and it increased to 0.81 about 3 years after the event. Pile group configuration and pile-to-pile distance can significantly influence the bending moment of piles [28]. Previously, conventional group pile foundations were used for moderately high buildings. Recently, Garg and Sawant [9] investigated the contribution of load sharing to vertical load for different CPRF configurations. Chanda et al. [6] summarised the studies on CPRFs subjected to seismic loads using static and dynamic approaches.

Based on the literature review, it is observed that mostly studies have used either 2×2 CPRF or 3×3 CPRF. However, limited studies have used higher pile group configurations for CPRF. Hence, the aim of this study is to determine the CPRF coefficient of pile rafts using higher pile group configurations under axial loading conditions. In the study, 5×5 and 7×7 pile groups are considered. The numerical study by Kumar et al. [15] and experimental investigations by Horikoshi et al. [10, 11] initially simulated a 2×2 pile raft system in PLAXIS3D for static loading conditions to validate the results. The model is modified for higher pile group configurations (5×5 and 7×7) after successful validation with available field-measured results. Further, a parametric study is performed on 5×5 and 7×7 CPRFs to investigate the effects of yield criteria, pile length, raft thickness, friction angle, soil modulus, and different pile group configurations. The results of this study can be beneficial in the practical design of such foundations, particularly for the construction of high-rise buildings.

2. NUMERICAL MODELLING AND VALIDATION

Initially, a soil model with dimensions 28 m × 28 m × 16 m is created using 10 node tetrahedral elements. The Mohr-Coulomb constitutive model was used to model Toyoura sand. A square raft of width 4 m and thickness 1 m is modelled using plate elements. Four fixed-head piles, with diameter D=500 mm and length $L=9$ *m*, are modelled using the volume pile element. The centre-to-center pile spacing is 2 m. A medium-sized mesh with 21,627 soil elements and 35,550 nodes with an average element size of 0.5 cm is generated. Figure 1 shows the discretised finite element mesh of CPRF. All other subsequent analyses derived from this element are provided in Appendix as Supplementary Material (Figure A1-A4). The properties of Toyoura sand, piles, and rafts have been reported by Horikoshi et al. [10, 11], Eslami et al. [7], and Kumar et al. [15]. These properties are listed in Table 1. The load applied to the model is 5862.5 kN, corresponding to a raft weight of 4.69 kg at a centrifugal acceleration of 50 g, as reported by Horikoshi et al. [10, 11]. Vertical loading in the form of surface load is applied on the top of CPRF. The total vertical load shared by piles is approximately 3018.355 kN, and hence, the CPRF coefficient of piles is obtained as 0.515, which is in good agreement with the CPRF value of 0.47 as reported by Kumar et al. [15]. However, here a pile shares the maximum proportion of the load. Figure A1 shows a vertical displacement contour which has a maximum value of 21.87 mm, which is in good agreement with the value of 15 mm as reported by Horikoshi et al. [11]. Table 1 shows the properties adopted in this study.

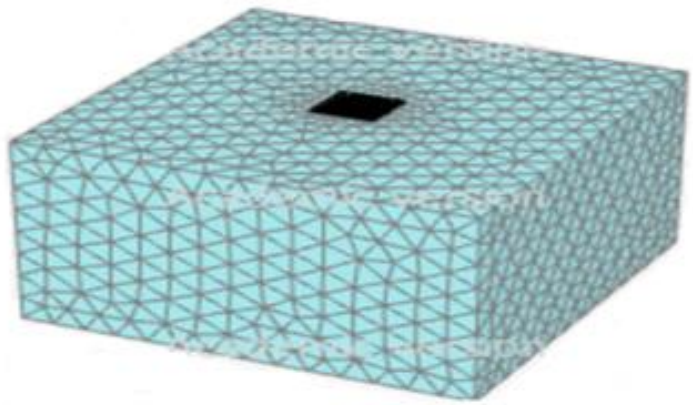

Figure 1 Discretized mesh of CPRF

Table 1 Properties used in present study [7, 10, 11, 15]

Properties	Soil	Pile	Raft
Material	Toyoura Sand	Concrete	Aluminium
Young's Modulus (MPa)	40	41700	70000
Poisson's ratio (μ)	0.3	0.2	0.35
Unit weight (kN/m^3)	16.3	24	27
Friction Angle (φ)	31	-	-
Dilation Angle (ψ)	1	-	-
Cohesion (kN/m^2)	10	-	-

3. PARAMETRIC STUDY

To minimise the boundary effects, a convergence study has been performed to fix boundary size. The dimension of the soil model has been fixed as 70 m × 70 m in plan and vertical dimension Z_p for higher pile group configurations. The value of Z_p depends on the pile length to have a certain distance between the pile tip and the bottom boundary. Here the elastic modulus of soil is considered as 60,000 kPa. Piles considered in the study are modelled as volume elements. Piles considered in the study are modelled as volume elements. Pile diameter D is constant at 0.5 m. Usually, in construction, a raft is made up of concrete; hence, the material of the raft is modified to concrete with an elastic modulus of 41.7 GPa, Poisson's ratio of 0.2 and unit weight of 24 kN/m^3. Length L, raft thickness R_t, friction angle Φ and soil modulus E are considered variables in the parametric study. Furthermore, the raft is placed at a depth of 1 m below ground level, as the depth of the raft should not be less than 1 m [10].

For 5 × 5 CPRF, a square raft with a width of 10 m and a thickness of 1 m is modelled using plate elements. A medium-sized mesh is generated with 1,05,420 soil elements and 1,68,773 nodes having an average element size of 0.5 cm. The load applied to the model is 110.2 MN. Figure A2 shows a schematic view of the 5×5 CPRF and discretised finite element mesh of CPRF. The piles in the group are placed with a centre-to-centre spacing of 4D. Offset between the edge of the raft and the outermost pile is 1 m. Here, the pile shares the maximum proportion of the load. For the 7 × 7 CPRF, the team models a square raft with a width of 14 m and a thickness of 1 m using plate elements. A medium-sized mesh is generated with 1,97,296 numbers of soil elements and 3,16,728 numbers of nodes, having an average element size of 0.5 cm. The load applied to the model is 216 MN. Figure A4 shows a schematic view of a 7×7 CPRF and discretised finite element mesh of CPRF. Piles in the group are placed with a center-to-center spacing of 4D. Offset between the edge of the raft and the outermost pile is 1 m. Total vertical resistance provided by piles is 125586 kN, which is obtained by the summation of axial forces at different pile heads. CPRF coefficients of pile and raft are 0.581 and 0.419, respectively. Here a pile shares the maximum proportion of load.

Figure A3 shows the vertical displacement contours (L = 9 m), which have maximum values of 196 mm and 228 mm for 5 × 5 and 7 × 7 CPRF, respectively. Figure 5 shows the axial force variation along the pile length. From the graph, it can be observed that axial force is maximum at the pile head, and then it decreases due to skin friction offered to the pile from surrounding soil. For 7 × 7 CPRF, the force at the top of the pile is 2671.7 kN, which has been dropped to 1176.3 kN at the tip of the pile. This suggests an end-bearing resistance of 1176.3 kN and a shaft resistance of 1495.3 kN. Similarly for 7 × 7 CPRF, the force at the top of the pile is 2837.7 kN, which has been dropped to 1268.181 kN at the pile tip. This suggests an end-bearing resistance of 1268.2 kN and a shaft resistance of 1569.5 kN. Figure 6 shows the variation in the vertical stress at the centre of the raft.

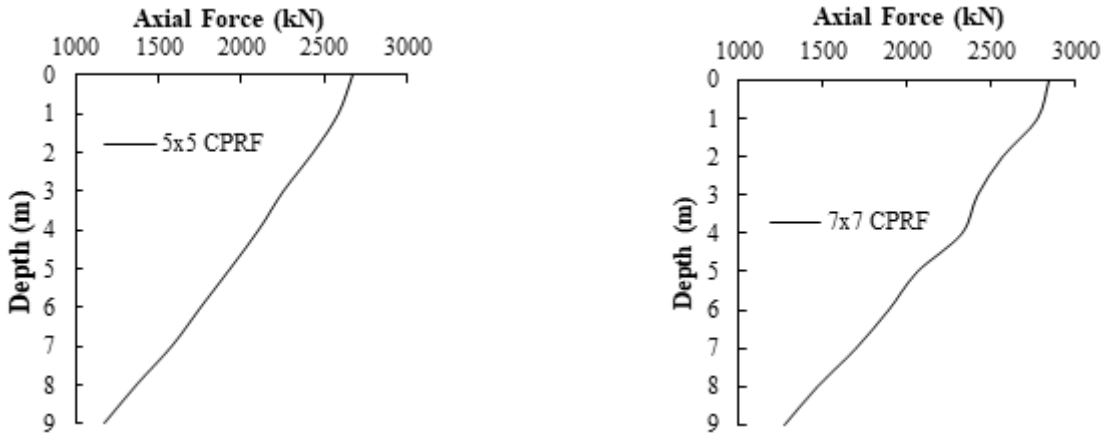

(a) 5×5 CPRF (b) 7×7 CPRF

Figure 2 Axial force variation for along pile length

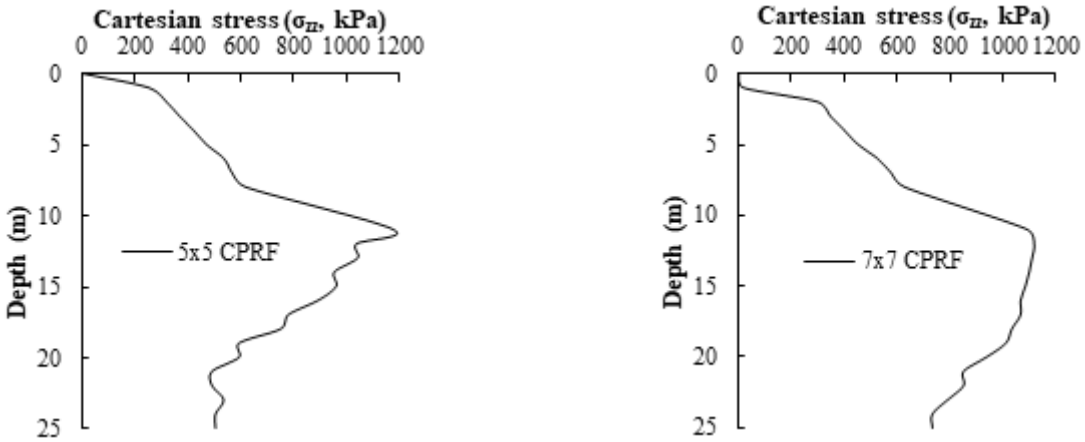

(a) 5×5 CPRF (b) 7×7 CPRF

Figure 3 Variation in stress, σ_{zz} with depth at centre of CPRF

3.1. Effect of Yield Criteria

A comparative analysis of the Mohr-Coulomb model (MC model) and the Hardening Soil model (HS model) is performed to investigate the impact of yield criteria on the response of CPRF. The Mohr-Coulomb model is a fundamental model for linear elastic perfectly plastic behaviour in soils. It is characterised by Hooke's law for elastic deformation and the Mohr-Coulomb failure criterion for plastic yielding. The MC model, which represents linear elastic-perfectly plastic behaviour, requires five parameters (c, φ, ψ, E, μ) that are widely used in practical applications. The HS model offers a more sophisticated representation of soil behaviour by encompassing a wider range of soil types, from stiff to soft. The model incorporates stress-dependent stiffness, plastic straining due to primary deviatoric loading, primary compression and elastic unloading/reloading behaviour and the Mohr-Coulomb failure criterion (c, φ, ψ). An empirical method suggested by Brinkgreve et al. [3] was employed to calculate sand parameters at a relative density of 32.5%. The parameters employed for this study are presented in Table 2.

In the case of 5×5 CPRF, with an applied load of 110.2 MN, the total vertical resistance offered by the piles is 70248.8 kN, obtained by summing the axial forces at different pile heads. Therefore, the CPRF coefficients for the pile and raft are 0.637 and 0.363, respectively. Here, the pile shares the maximum proportion of the load. In comparison to MC yield criteria, the CPRF coefficient of piles increases while that of the raft decreases in case of HS yield criteria. Figure A4 shows the vertical displacement contours (L = 9 m), which have a maximum value of 430.8 mm.

Table 2 Parameters of soil for HS model [3]

Parameters	Value
Secant elastic modulus, E_{50}^{ref} (kPa)	600 × D_r %
Odometer elastic modulus, E_{oed}^{ref} (kPa)	E_{50}^{ref}
Unloading-reloading elastic modulus, E_{ur}^{ref} (kPa)	$3E_{50}^{ref}$
Rate of stress dependency, m	0.7 – (D_r %/320)
Failure ratio, R_f	1 – (D_r %/800)
Poisson's ratio (μ_{ur})	0.2

The settlement of CPRF increases with the HS yield criteria in comparison to the MC yield criteria. Figure 4(a) shows the axial force variation along the pile length for MC as well as HS yield criteria. From the graph, it can be observed that axial force is maximum at the pile head, and then it decreases due to skin friction offered to the pile from surrounding soil. In the case of HS yield criteria, the force at the top of the pile is 3258.604 kN, which has been dropped to 1513.453 kN at the tip of the pile. This suggests an end-bearing resistance of 1513.453 kN and a shaft resistance of 1745.151 kN. Since the HS yield criteria are stiffer than the MC yield criteria, the axial force in the former case is greater than in the latter one, which implies a higher CPRF coefficient in the HS yield criteria.

In the case of 7×7 CPRF, corresponding to the applied load of 216 MN, the total vertical resistance offered by piles is 145380 kN, which is obtained by the summation of axial forces at different pile heads, and hence the CPRF coefficients of pile and raft are 0.673 and 0.327, respectively. Here the pile shares the maximum proportion of a load. In comparison to MC yield criteria, the CPRF coefficient of piles increases, while that of piles decreases in the case of HS yield criteria. The vertical displacement contours (L = 9 m), which have a maximum value of 479.6 mm (Figure A4). The settlement of CPRF increases with the HS yield criteria in comparison to the MC yield criteria. Figure 4(b) shows the axial force variation along the pile length for MC as well as HS yield criteria. From the graph, it can be observed that axial force is maximum at the pile head, and then it decreases due to skin friction offered to the pile from surrounding soil. In the case of HS yield criteria, the force at the top of the pile is 3451.63 kN, which has been dropped to 1691.14 kN at the tip of the pile. This suggests an end bearing resistance of 1691.138 kN and a shaft resistance of 1760.49 kN. Since the HS yield criterion is stiffer than the MC yield criteria, the axial force in the former case is greater than in the latter one, which implies a higher CPRF coefficient in the HS yield criteria.

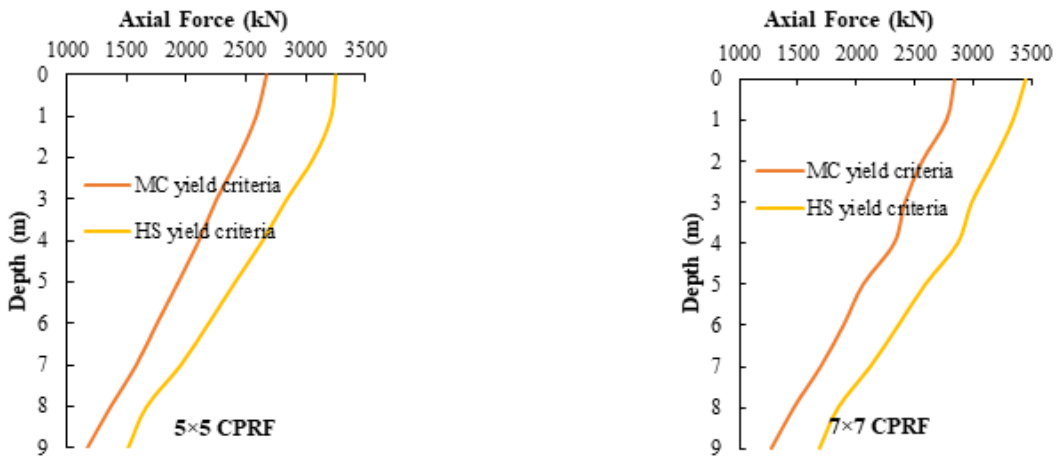

(a) 5×5 CPRF (b) 7×7 CPRF

Figure 4 Comparison of axial force variation with different yield criteria for 5×5 and 7×7 CPRF

3.2. Effect of *L/D* Ratio

The pile length is varied from 9 m to 20 m. However, the diameter is kept constant as 0.5 m. The L/D ratio is therefore adjusted between 18 and 40. The results of the 5×5 CPRF are shown in Table 3. With the increase in the *L*/*D* ratio, the CPRF coefficient of the raft and settlement of CPRF decrease while the CPRF coefficient of the pile increases. With the increase in *L*/*D* ratio, pile stiffness increases, and hence, settlement decreases. Figure 5 shows the axial force variation with respect to different *L*/*D* ratios. From the graph, it can be observed that with the increase in *the L/D ratio, the* axial load of piles increases, and hence the pile CPRF coefficient increases. It can also be observed that maximum axial force is obtained at the pile head. Total load shared by a single pile varies from 2671.7 kN (*L*/*D* = 18) to 3549.9 kN (*L*/*D* = 40). End-bearing resistance varies between 1176.3 kN and 1240.1 kN. Shaft resistance is almost parabolically varying with pile length (Figure 6) from 1495.3 kN (*L*/*D* = 18) to 2475.7 kN (*L*/*D* = 40).

Figure 7 shows the variation of the CPRF coefficient of piles and raft with applied vertical load for a 5×5 CPRF at pile lengths of 9 m and 20 m, respectively. For CPRF with *L* = 9 m, the CPRF coefficient of the raft increases with load level from 0.268 to 0.446. It increases with the load level from 0.144 to 0.259 (*L* = 20 m). On the other hand, the CPRF coefficient of pile decreases with load level from 0.732 to 0.554 for CPRF with *L* = 9 m. It decreases with the load level from 0.856 to 0.741 (L = 20 m). From the graphs, it can be observed that the CPRF coefficient of piles is higher during the initial stage and that of rafts is lower. Initially, the majority of the load is transferred to the pile. A small vertical movement of the pile is required to mobilise skin friction, whereas considerably greater settlement is essential to mobilise the ultimate bearing capacity of the soil below the raft. Then, the CPRF coefficient of piles decreases nonlinearly with the increase in load as the proper interaction between soil and raft gets established. It can also be observed that the CPRF coefficient for piles is higher at a length of 20 m compared to a length of 9 m, while the CPRF coefficient for the raft shows the opposite trend.

Table 3 CPRF Coefficient and Settlement for different *L*/*D* ratio for 5×5 CPRF

L/D	CPRF Coefficient		Settlement (mm)	Total Load on Pile, *Q* (kN)	End Bearing, Q_b (kN)
	Piles	Raft			
18	0.554	0.446	196.2	2671.665	1176.333
20	0.585	0.415	189.1	2850.806	1240.149
22	0.612	0.388	178.4	2978.324	1190.634
24	0.635	0.365	169.1	3045.189	1194.59
26	0.656	0.344	157.9	3140.763	1195.561
28	0.675	0.325	149.3	3212.679	1175.416
30	0.694	0.306	139.2	3329.01	1169.087
32	0.704	0.296	128	3365.449	1163.985
36	0.726	0.274	106.7	3467.374	1084.261
40	0.741	0.259	85.56	3549.876	1074.307

Similarly, the results of the 7×7 CPRF are summarised in Table 4. With the increase in *L*/*D* ratio, the CPRF coefficient of raft and settlement of CPRF decreases while the CPRF coefficient of pile increases. With the increase in the *L*/*D* ratio, the load-carrying capacity of the pile increases. With this overall stiffness of the pile configuration increases, resulting in a decrease in the settlement. Figure 8 shows the axial force variation for different *L*/*D* ratios. From the graph, it can be observed that with an increase in *the L/D ratio, the* axial load of piles increases, and hence the CPRF coefficient of piles increases. It can also be observed that maximum axial force is obtained at the pile head. The total load shared by a single pile varies from 2837.7 kN (*L*/*D* = 18) to 3770.4 kN (*L*/*D* = 40). End-bearing resistance varies between 1221.0 kN and 1298.6 kN. Shaft resistance is almost parabolically varying with pile length (Figure 9) from 1569.5 kN (*L*/*D* = 18) to 2549.4 kN (*L*/*D* = 40).

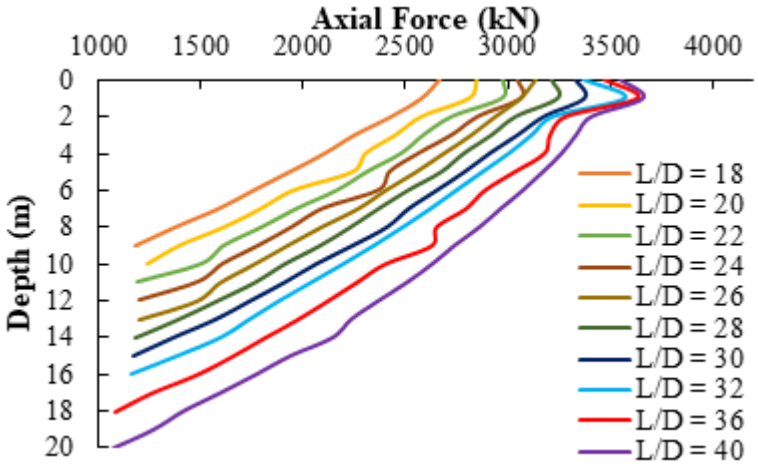

Figure 5 Axial force variation along depth for different *L*/*D* ratio of 5×5 CPRF

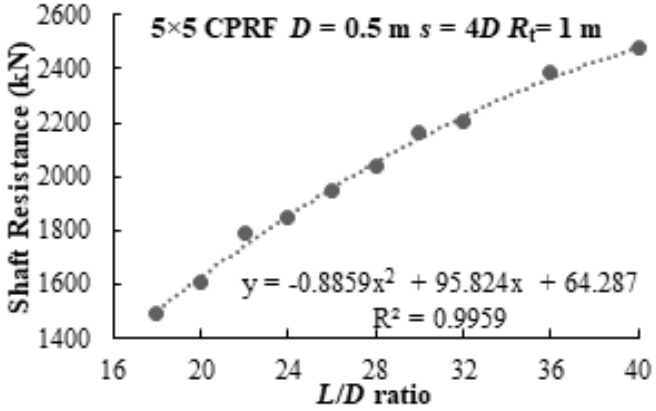

Figure 6 Variation in Shaft resistance with *L*/*D* ratio for 5×5 CPRF

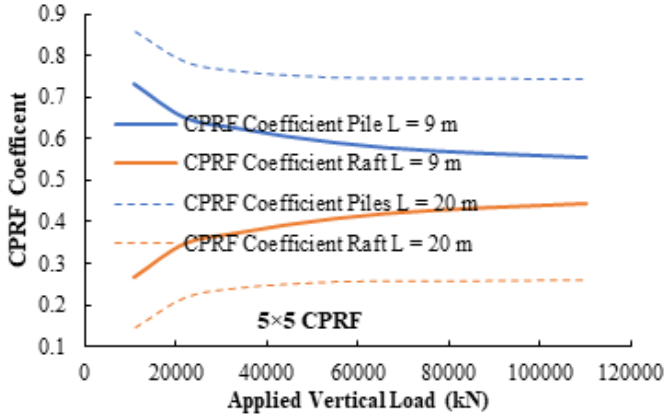

Figure 7 Variation of CPRF Coefficient of piles and raft for 5×5 CPRF at *L* = 9 m and *L* = 20 m

The variations in CPRF coefficient of piles and rafts (Figure 10) with applied vertical load for 7×7 CPRF at pile lengths of 9 m and 20 m, respectively. For CPRF with *L* = 9 m, the CPRF coefficient of the raft increases with load level from 0.227 to 0.419 It increases with load level from 0.111 to 0.233 (*L* = 20 m). On the other hand, the CPRF coefficient of the pile decreases with load level from 0.773 to 0.581 for CPRF with *L* = 9 m. It decreases with load level from 0.889 to 0.767 (*L* = 20 m). From the graphs, it can be observed that the CPRF coefficient of piles is higher during the initial stage than that of rafts. Initially, most of the load is transferred to the pile. A small vertical movement of the pile is required to mobilise skin friction, whereas considerably greater settlement is essential to mobilise the ultimate bearing capacity of the raft. Then, the CPRF coefficient of piles decreases non-linearly with the increase in load as the proper interaction between soil and raft gets established. It can also be observed that the

CPRF coefficient for piles is higher at a length of 20 m compared to a length of 9 m, while the CPRF coefficient for the raft shows the opposite trend.

Table 4 CPRF Coefficient and Settlement of 7×7 CPRF for different *L*/*D* ratio

L/D	CPRF Coefficient		Settlement (mm)	Total Load, *Q* (kN)	End Bearing, Q_b (kN)
	Piles	Raft			
18	0.581	0.419	228.3	2837.721	1268.181
20	0.612	0.388	217.4	2989.489	1282.544
22	0.642	0.358	205.8	3094.193	1276.744
24	0.666	0.334	194.3	3166.195	1298.587
26	0.688	0.312	182.4	3330.211	1293.856
28	0.718	0.282	170.6	3459.023	1274.604
30	0.726	0.274	158	3452.895	1247.855
32	0.736	0.264	144.5	3480.526	1246.539
36	0.756	0.244	120.7	3647.098	1233.408
40	0.767	0.233	96.34	3770.43	1221.037

In the case of vertical loading, the pile CPRF coefficient is higher, which implies higher load sharing. The pile CPRF coefficients, α_{Pile} for 5×5 CPRF and 7×7 CPRF are 0.554 and 0.581, respectively. With the increase in the number of piles, the CPRF coefficient, α_{Pile} varied marginally, which implies little influence of the pile group upon the CPRF coefficient. However, it has a significant influence on settlement, as with the increase in the size of a pile-raft, settlement of CPRF also increases under the same vertical load per unit area (1.1 MPa). Settlement of 5×5 CPRF and 7×7 CPRF are 196.2 mm and 228.3 mm, respectively, which implies that the settlement of 7×7 CPRF is more than the settlement of 5×5 CPRF by 16.36%. It is to be noted that elastic settlement S_e of a square foundation under surcharge q varies linearly with the width of foundation B [2] as, $S_e = I_f \times qB(1 - \mu_s{}^2)/E_s$. For 7×7 CPRF, the width of the raft is 14 m (40% more). But the absolute value of the settlement is just increased by 16.36%. If absolute settlements are normalised for the width of foundation *B*, the normalised value decreases for higher CPRF configurations.

The effect of *the L/D* ratio is prominent. With an increase in *L*/*D* ratio, the settlement of CPRFs decreases. which implies a reduction in settlement. The settlement decreases from 196.2 mm to 85.56 mm, corresponding to *L*/*D* = 18 to 40 for 5×5 CPRF, which implies a 56.4% reduction in settlement. Similarly, for the 7×7 CPRF, the settlement decreases from 228.3 mm to 96.3 mm, corresponding to L/D values of 18 to 40, which implies a 57.8% reduction in settlement. The CPRF coefficient of piles increases and that of rafts decreases with an increase in *the L/D* ratio. The CPRF coefficient of piles increases from 0.554 to 0.741, corresponding to *L*/*D* = 18 to 40 for 5×5 CPRF, which implies a 33.7% increment in the CPRF coefficient of piles. Similarly for 7×7 CPRF, the CPRF coefficient increases from 0.581 to 0.767, corresponding to *L*/*D* = 18 to 40, which implies a 32.0% increment in the CPRF coefficient of piles. Initially the CPRF coefficient of piles is higher and that of rafts is lower. A small vertical movement of the pile is required to mobilise skin friction; hence, more contribution of piles. Thereafter, the CPRF coefficient of piles decreases non-linearly with the increase in load as the proper interaction between soil and raft gets established.

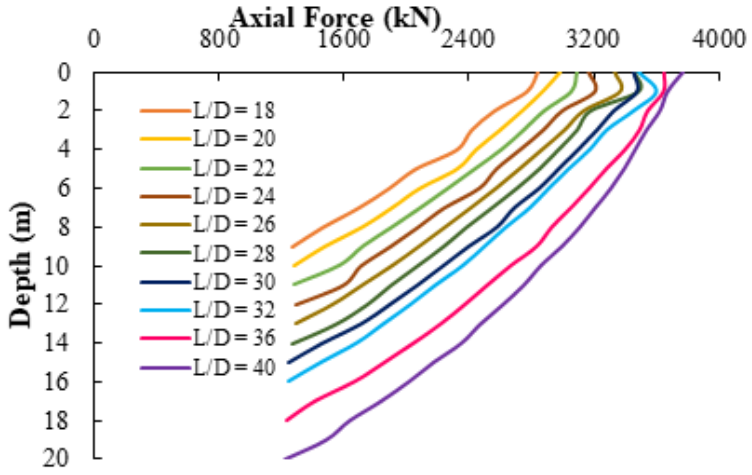

Figure 8 Axial force variation along depth for different *L*/*D* ratio of 7×7 CPRF

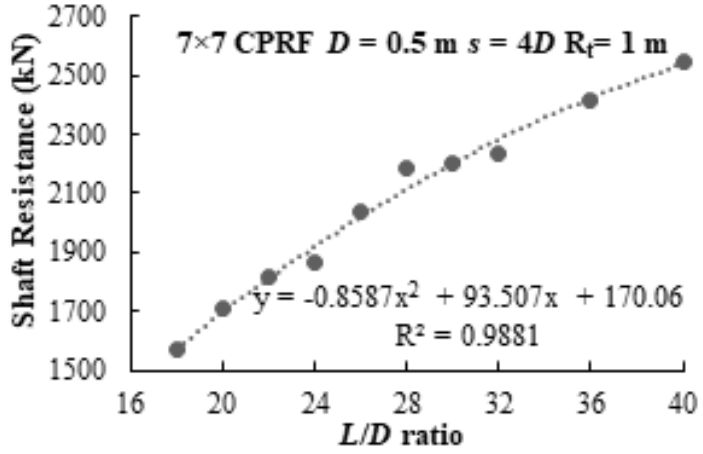

Figure 9 Variation in shaft resistance with *L*/*D* ratio for 7×7 CPRF

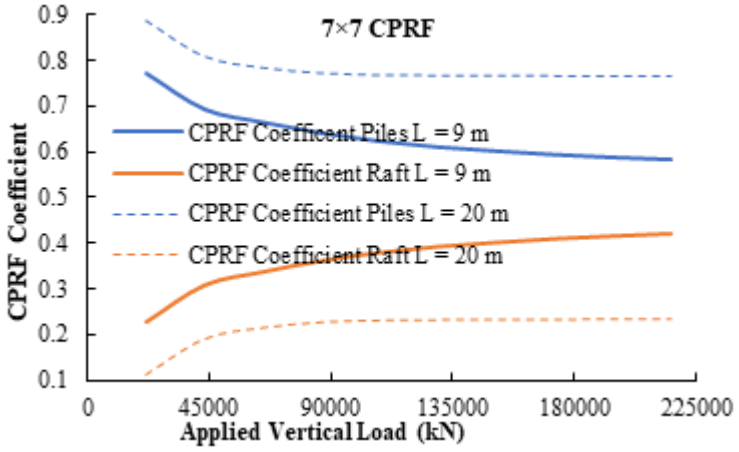

Figure 10 Variation of CPRF Coefficient of piles and raft for 7×7 CPRF at *L* = 9 m and *L* = 20 m

3.3. Effect of R_t/B

Here raft thickness is varied from 1 m to 2.5 m. However, width is kept constant. The results of the same are shown in Table 5. With the increase in the raft thickness, settlement of CPRF increases due to an increase in the self-weight of the raft. This observation is similar to that reported by Sawant and Ladhane [22]. However, the CPRF coefficient remains constant for a given pile length at any raft thickness. Figure 11(a) shows the variation of axial force along the depth of 5×5 CPRF with respect to different R_t/B for a particular pile length. From the graphs, it

can be observed that maximum axial force is developed at the head of piles. It decreases with depth due to mobilised friction in the surrounding soil. Figure 12(a) shows the variation of load on piles with R_t/B for 5×5 CPRF. From the graph it can be observed that there is a marginal increase of load on piles with an increase in raft thickness; hence, the CPRF coefficient of piles and raft are almost constant.

Table 5 Settlement of 5×5 CPRF for different R_t/B and pile length

R_t/B	Vertical Settlement (mm)									
	***L*=9m**	***L*=10m**	***L*=11m**	***L*=12m**	***L*=13m**	***L*=14m**	***L*=15m**	***L*=16m**	***L*=18m**	***L*=20m**
0.1	196.2	189.1	178.4	169.1	157.9	149.3	139.2	128	106.7	85.56
0.15	198.5	191.5	180.8	171.2	160	151.3	140.8	129.7	108.1	86.83
0.175	199.7	192.7	181.9	172.3	161.1	152.4	141.7	130.6	108.9	87.47
0.2	200.9	194	183	173.4	162.1	153.4	142.7	131.5	109.6	88.11
0.225	202.1	195.2	184.2	174.5	163.2	154.3	143.6	132.3	110.4	88.74
0.25	203.3	196.4	185.4	175.7	164.2	155.3	144.4	133.2	111.1	89.34

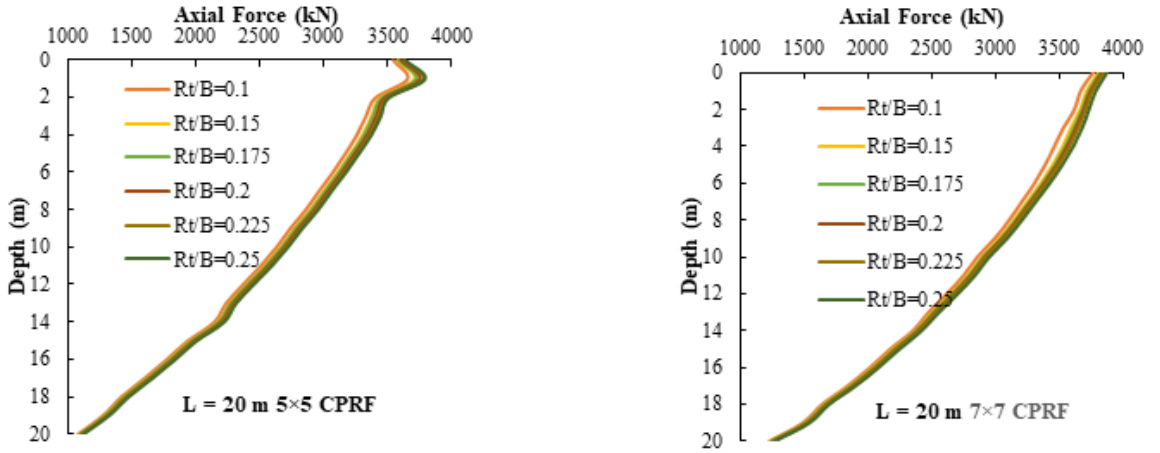

(a) 5×5 CPRF (b) 7×7 CPRF

Figure 11 Axial force variation along depth for different R_t/B of 5×5 and 7×7 CPRF

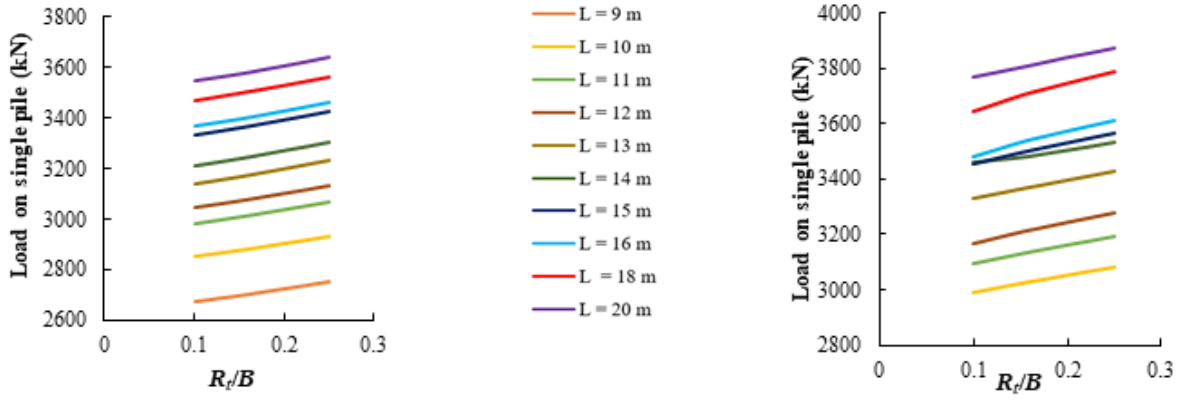

(a) 5×5 CPRF (b) 7×7 CPRF

Figure 12 Variation of load on piles with R_t/B for 5×5 and 7×7 CPRF

Similarly, the response of the 7×7 CPRF is reported in Table 6 in the form of vertical settlement. With the increase in the raft thickness, settlement of CPRF increases due to the increase in self-weight of the raft. This observation

is like that reported by Teji and Ashango [24]. However, the CPRF coefficient varies marginally with changes in the raft thickness. Figure 11(b) shows the variation of axial force along the depth of a 7×7 CPRF for different R_t/B values at a specific pile length. From the graphs, it can be observed that maximum axial force is obtained at the head of piles. Figure 12(b) shows the load variation on piles with R_t/B for 7×7 CPRF. From the graph, it can be observed that there is a marginal increase of load on piles with the increase in raft thickness; hence, the CPRF coefficient of piles and raft is almost constant. As raft thickness increases, CPRF settlement rises due to the raft's increased dead weight and rigidity. Flexural rafts exhibit bending deformations with some load sharing and approximately uniform pressure distribution. However, the CPRF coefficient remains almost constant with an increase in raft thickness, which implies that the CPRF coefficient is independent of raft thickness.

Table 6 Settlement of 7×7 CPRF for different R_t/B and pile length

R_t/B	Vertical Settlement (mm)									
	***L*=9m**	***L*=10m**	***L*=11m**	***L*=12m**	***L*=13m**	***L*=14m**	***L*=15m**	***L*=16m**	***L*=18m**	***L*=20m**
0.1	228.3	217.4	205.8	194.3	182.4	170.6	158	144.5	120.7	96.34
0.15	230.8	220.3	208.9	196.5	184.5	172.8	159.4	146.4	121.9	97.44
0.175	232.0	221.6	210.2	197.7	185.5	173.8	160.3	147.3	122.6	98.01
0.2	233.3	222.8	211.3	198.8	186.6	174.8	161.1	148.2	123.3	98.54
0.225	234.5	224	212.6	199.8	187.7	175.8	162	149	124	99.19
0.25	235.7	225.2	213.7	200.8	188.6	176.8	162.9	149.9	124.7	99.81

3.4. Effect of Friction Angle

The soil friction angle is varied from Φ = 31° to Φ = 39°. Load settlement responses of 5×5 CPRF at these friction angles are presented in Figure 13. From the graph, it can be observed that the CPRF settlement decreases with an increase in friction angle. This is due to an increase in the shaft resistance associated with soil friction angle. Table 7 shows CPRF coefficients and vertical settlement of 5×5 CPRF under vertical load 110204 kN corresponding to different friction angles. With the increase in friction angle, the CPRF coefficient of the pile decreases from 0.741 (Φ=31°) to 0.733 (Φ=39°) and that of raft increases from 0.259 (Φ=31°) to 0.267 (Φ=39°). This reduction can be attributed to the increase in the bearing capacity of the raft. Settlement of CPRF decreases from 85.56 mm (Φ=31°) to 71.83 mm (Φ=39°) with the increase in friction angle. It implies a 16.05% reduction in settlement for 5×5 CPRF.

Table 7 CPRF Coefficients and Settlement of 5×5 CPRF and 7×7 CPRF for different Friction angles

Friction Angle (°)	CPRF Coefficient 5×5		Settlement 5×5 (mm)	CPRF Coefficient 7×7		Settlement 7×7 (mm)
	Piles	Raft		Piles	Raft	
31	0.741	0.259	85.56	0.767	0.233	96.34
33	0.740	0.260	81.16	0.765	0.235	92.11
35	0.738	0.262	77.50	0.763	0.237	88.58
37	0.736	0.264	74.45	0.762	0.238	85.71
39	0.733	0.267	71.83	0.759	0.241	83.20

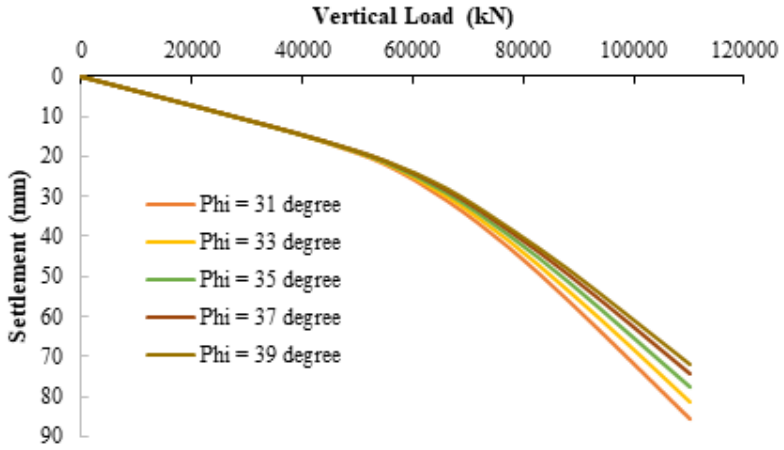

Figure 13 Load settlement curve for 5×5 CPRF at different friction angles

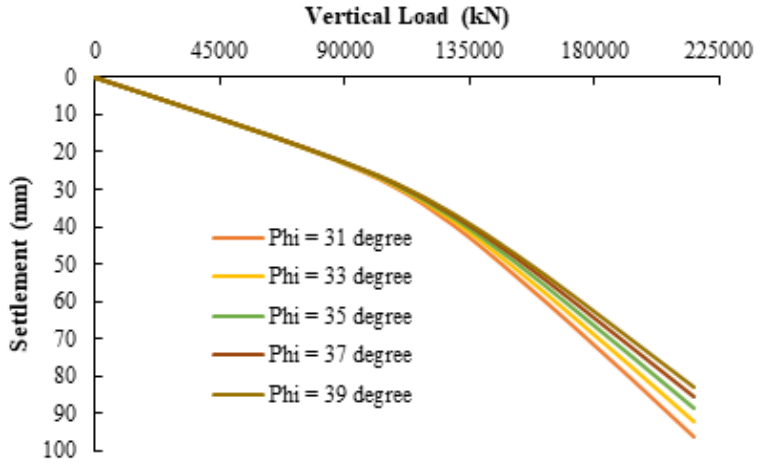

Figure 14 Load settlement curve for 7×7 CPRF at different friction angles

The load settlement responses of 7×7 CPRF for different friction angles are presented in Figure 14. From the graph, it can be observed that with the increase in friction angle, settlement of CPRF decreases. This is due to an increase in the shaft resistance associated with soil friction angle. Table 7 also shows CPRF coefficients and vertical settlement of 7×7 CPRF under vertical load 216000 kN corresponding to different friction angles. With the increase in friction angle, the CPRF coefficient of the pile decreases from 0.767 (Φ=31°) to 0.759 (Φ=39°), and that of the raft increases from 0.233 (Φ=31°) to 0.241 (Φ=39°). Settlement of CPRF decreases from 96.34 mm (Φ=31°) to 83.20 mm (Φ=39°) with an increase in friction angle. This implies a 13.64% reduction in settlement owing to an increase in shaft resistance. It can be concluded that the CPRF coefficient of piles decreases and that of rafts increases with an increase in friction angle.

3.5. Effect of E_s/E_p

The soil modulus, E_s, of dense sand is 81,000 kPa according to Bowles [2]. Hence, the soil modulus, E_s, is varied from 60,000 kPa to 81,000 kPa here. However, the pile's modulus of elasticity is kept constant. Table 8 reports the values of different E_s/E_p and pile lengths for 5×5 and 7×7 CPRF. Figures 15 and 16 show the settlement variation with E_s/E_p for different pile lengths, for 5×5 and 7×7, respectively. The settlement of CPRF decreases with an increase in E_s/E_p. The rate of decrease in settlement decreases as the E_s/E_p increases. This phenomenon can be attributed to the behaviour of soil-CPRF as a unit system. In fact, in the case of stiff soil CPRF behaves as if it were located on a very thick foundation. The CPRF coefficients of piles and rafts are almost constant with respect to variation in E_s/E_p. Soil modulus contributes to the soil stiffness of a raft and pile simultaneously. This can alter nearly the same alteration in the stiffness of the raft and piles, resulting in nearly the same load sharing. The CPRF coefficient of piles increases from 0.554 (L=9 m) to 0.741 (L=20 m) for 5×5 CPRF. Similarly, it increases from

0.581 (L=9 m) to 0.767 (L=20 m) for 7×7 CPRF. Table 9 summarises the CPRF coefficients of piles and rafts for different pile lengths for 5×5 CPRF as well as 7×7 CPRF.

Table 8 Settlement of 5×5 and 7×7 CPRF for different E_s/E_p and pile length

E_s/E_p	Vertical Settlement (mm) of 5×5 CPRF (mm)									
	L=9m	L=10m	L=11m	L=12m	L=13m	L=14m	L=15m	L=16m	L=18m	L=20m
0.00144	196.2	189.1	178.4	169.1	157.9	149.3	139.2	128	106.7	85.56
0.00151	187	180.1	170.1	161.1	150.5	142.3	132.7	122.1	101.7	81.65
0.00158	178.5	172	162.4	153.9	143.8	135.9	126.7	116.6	97.19	78.09
0.00166	170.8	164.5	155.3	147.3	137.6	130.1	121.3	111.7	93.08	74.84
0.00173	163.8	157.7	148.9	141.2	131.9	124.8	116.4	107.1	89.31	71.83
0.0018	157.3	151.5	143	135.6	126.7	119.9	111.8	102.9	85.86	69.11
0.00187	151.3	145.7	137.6	130.5	121.9	115.3	107.6	99.01	82.66	66.57
0.00194	145.7	140.3	132.5	125.7	117.4	111.1	103.7	95.42	79.65	64.23
	Vertical Settlement (mm) of 7×7 CPRF (mm)									
0.00144	228.3	217.4	205.8	194.3	182.4	170.6	158	144.5	120.7	96.34
0.00151	217.5	207	196	185.1	173.8	162.5	150.6	137.8	115.1	91.95
0.00158	207.7	197.7	187.1	176.8	166	155.3	143.9	131.6	110	87.94
0.00166	198.7	189.1	179	169.2	158.9	148.6	137.8	126	105.4	84.30
0.00173	190.4	181.2	171.6	162.2	152.3	142.5	132.1	120.9	101.1	80.95
0.0018	182.8	174	164.7	155.8	146.3	136.9	127	116.1	97.21	77.87
0.00187	175.8	167.3	158.4	149.9	140.7	131.7	122.2	111.8	93.59	75.03
0.00194	169.3	161.2	152.5	144.4	135.5	126.9	117.7	107.7	90.26	72.40

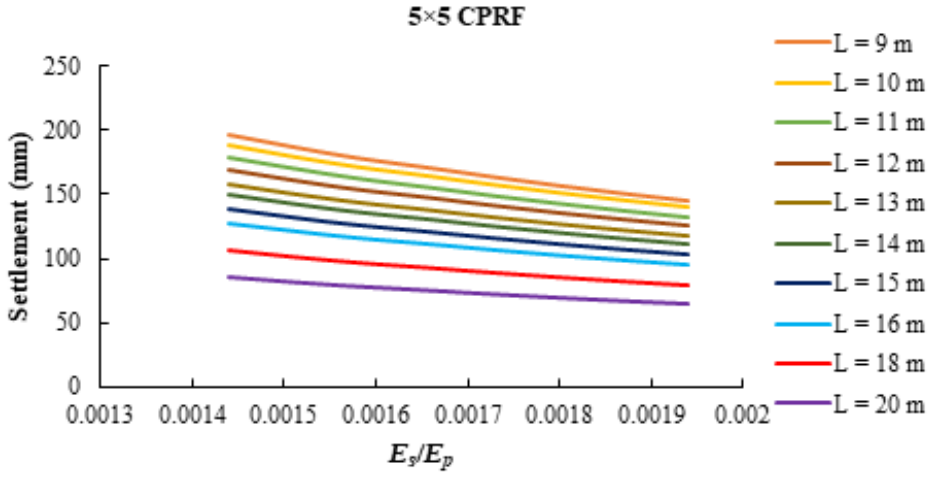

Figure 15 Variation in settlement with soil modulus for 5×5 CPRF at different E_s/E_p

Table 9 CPRF Coefficient of Pile and Raft for 5×5 CPRF and 7×7 CPRF for different pile lengths

CPRF Coefficient	*L*=9m	*L*=10m	*L*=11m	*L*=12m	*L*=13m	*L*=14m	*L*=15m	*L*=16m	*L*=18m	*L*=20m
5×5 Pile	0.554	0.585	0.612	0.635	0.656	0.675	0.694	0.704	0.726	0.741
5×5 Raft	0.446	0.415	0.388	0.365	0.344	0.325	0.306	0.296	0.274	0.259
7×7 Pile	0.581	0.612	0.642	0.666	0.688	0.718	0.726	0.736	0.756	0.767
7×7 Raft	0.419	0.388	0.358	0.334	0.312	0.282	0.274	0.264	0.244	0.233

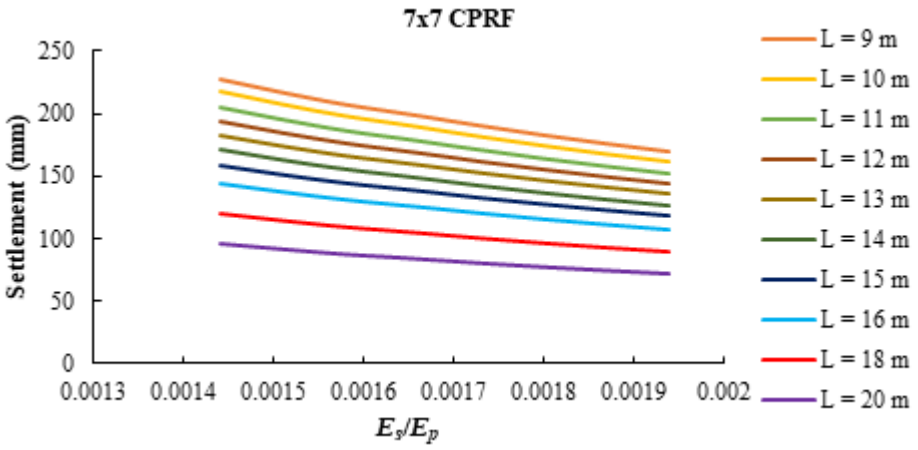

Figure 16 Variation in settlement with E_s/E_p for 7×7 CPRF at different pile lengths

4.0 CONCLUSIONS

Using PLAXIS-3D finite element software, the response of higher pile group configurations in the case of CPRF is studied. The pile has been modelled as a volume element, and the raft has been modelled as a plate element. The investigations are focused on the response of CPRF subjected to vertical load. Further, a parametric study is conducted to investigate the effects of yield criteria, pile length, raft thickness, and friction angle, which have been discussed in detail. These findings are useful for designing CPRFs in the case of high-rise buildings, as generally the contribution of a raft in sharing a load is often ignored due to the complex calculation of the CPRF coefficient, and the foundation is designed as a conventional pile group foundation alone. With these findings, the design of CPRF is optimised, which in turn will lead to better durability of the system, thereby making the foundation economical and effective. The following key observations can be concluded:

a) As compared to MC yield criteria, the CPRF coefficient of piles becomes higher, while that for rafts becomes lower under HS yield criteria.
b) As compared to MC yield criteria, settlement of CPRF increases under HS yield criteria.
c) The CPRF coefficient of the pile increases with pile length due to an increase in the shaft resistance. Consequently, the CPRF coefficient of the raft decreases with pile length.
d) With the increase in the pile length, the settlement of CPRF decreases while the CPRF coefficient of the pile increases.
e) With the increase in the raft thickness, settlement of CPRF increases. However, the CPRF coefficient remains almost constant irrespective of the raft thickness.
f) With the increase in pile length, the axial force shared by piles also increases, whereas it remains almost constant with variation in the raft thickness.
g) With the increase in friction angle, settlement of CPRF decreases on account of more frictional resistance. The CPRF coefficient of piles decreases, and that of rafts increases with an increase in friction angle. This may be attributed to an increase in the bearing capacity of soil at the level of the raft.

h) The CPRF coefficient of piles is higher at the initial stage than that of the raft. This increase can be attributed to the fact that small movements at the pile-soil interface are good enough to mobilise skin friction. Thereafter, it varies non-linearly, with the CPRF coefficient of piles decreasing and that of the raft increasing due to the establishment of proper interaction between the raft and the soil.
i) With the increase in soil modulus, the settlement of CPRF decreases. However, the CPRF coefficient remains constant irrespective of the soil modulus.
j) Though absolute settlement increases with higher configurations, normalised settlement decreases with respect to raft width.

Conflicts of Interest

The authors report that there are no competing interests to declare.

References

[1] Baziar, M. H., Rafiee, F., Azizkandi, A. S., and Lee, C. J. (2018). "Effect of Super-Structure Frequency on the Seismic Behavior of Pile-Raft Foundation using Physical Modeling." *Soil Dynamics and Earthquake Engineering* 104: 196-229. https://doi.org/10.1016/j.soildyn.2017.09.028

[2] Bowles, J. E. (1987). "Foundation Analysis and Design." *McGraw-Hill, Singapore.*

[3] Brinkgreve, R., Engin, E. and Engin, H., K. (2010). "Validation of Empirical Formulas to Derive Model Parameters for Sands." *International Conference of Numerical Methods in Geotechnical Engineering* 7: 137-142. https://doi.org/10.1201/b10551-25

[4] Chanda, D., Saha, R. and Haldar, S. (2020). "Behaviour of piled raft foundation in sand subjected to combined V-M-H loading." *Ocean Engineering* 216: 107596. https://doi.org/10.1016/j.oceaneng.2020.107596

[5] Clancy, P., and Randolph, M. F. (1993). "An Approximate Analysis Procedure for Piled Raft Foundations." *International Journal for Numerical and Analytical Methods in Geomechanics* 17: 849-869. https://doi.org/10.1002/nag.1610171203

[6] Diptesh Chanda, Rajib Saha, Sumanta Haldar, Deepankar Choudhury (2023). "State-of-the-art review on responses of combined piled raft foundation subjected to seismic loads using static and dynamic approaches." *Soil Dynamics and Earthquake Engineering* 169, 107869. https://doi.org/10.1016/j.soildyn.2023.107869

[7] Eslami, M. M., Aminikhah, A., and Ahmadi, M. M. (2011). "A Comparative Study on Pile Group and Piled Raft Foundations (PRF) Behavior under Seismic Loading." *Computational Methods in Civil Engineering* 2(2): 185-199.

[8] Firoj, M., and Maheshwari, B. K. (2022). "Effect of CPRF on Nonlinear Seismic Response of an NNP Structure Considering Raft-Pile-Soil-Structure-Interaction." *Soil Dynamics and Earthquake Engineering* 158: 1-17. https://doi.org/10.1016/j.soildyn.2022.107295

[9] Garg, A., Sawant, V.A. (2025). 'Effect of Different Configurations of Combined Pile-Raft Foundation on Vertical Load-Carrying Capacity and Load Sharing." *Indian Geotech J* (2025). https://doi.org/10.1007/s40098-025-01388-z

[10] Horikoshi, K., Matsumoto, T., Hashizume Y., Watanabe, T. and Fukuyama, H. (2003a). "Performance of Piled Raft Foundations Subjected to Static Horizontal Loading." *International Journal of Physical Modelling in Geotechnics* 3(2): 37-50. https://doi.org/10.1680/ijpmg.2003.030204

[11] Horikoshi, K., Matsumoto, T., Hashizume, Y. and Watanabe T. (2003b). "Performance of Piled Raft Foundations Subjected to Dynamic Loading." *International Journal of Physical Modelling in Geotechnics* 3(2): 51-62. https://doi.org/10.1680/ijpmg.2003.030205

[12] IS: 2950 (Part I). (1981). "Indian Standard Code of Practice for Design and Construction of Raft Foundations" *Bureau of Indian Standards, New Delhi.*

[13] Kang, M. A., Banerjee, S., Lee, F.-H., and Xie, H. P. (2012). "Dynamic Soil-Pile-Raft Interaction in Normally Consolidated Soft Clay during Earthquakes." *Journal of Earthquake and Tsunami* 6(3): 1250031-1-1250031-12. https://doi.org/10.1142/S1793431112500315

[14] Katzenbach, R., Bachmann, G., Boled-Mekasha, G., and Ramm, H. (2005). "Combined Pile-Raft Foundation (CPRF): An Approximate Solution for the Foundation of High-Rise Buildings." *Slovak Journal of Civil Engineering* 3: 19-29.

[15] Kumar, A., Choudhury, D., and Katzenbach, R. (2016). "Effect of Earthquake on Combined Pile-Raft Foundation." *International Journal of Geomechanics* 16(5): 04016013-1-04016013-16. https://doi.org/10.1061/(ASCE)GM.1943-5622.0000637

[16] Matsumoto, T., Fukumura, K., Pastsakorn, K., Horikoshi K. and Oki, A. (2004a). "Experimental and Analytical Study on Behaviour of Model Piled Rafts in Sand Subjected to Horizontal and Moment Loading." *International Journal of Physical Modelling in Geotechnics* 4(3): 1-19. https://doi.org/10.1680/ijpmg.2004.040301

[17] Matsumoto, T., Fukumura, K., Horikoshi, K. and Oki, A. (2004b). "Shaking Table Tests on Model Piled Rafts in Sand Considering Influence of Superstructures." *International Journal of Physical Modelling in Geotechnics* 4(3): 21-38. https://doi.org/10.1680/ijpmg.2004.040302

[18] Matsumoto, T., Nemoto H., Mikami, H., Yaegashi, K., Arau, T., and Kitiyodom, P. (2010). "Load Tests of Piled Raft Models with Different Pile Head Connection Conditions and Their Analyses." *Soils and Foundations* 50(1): 63-81. https://doi.org/10.3208/sandf.50.63

[19] Nguyen, D. D. C., Kim, D.-S., and Jo, S.-B. (2013). "Settlement of Piled Rafts with Different Pile Arrangement Schemes via Centrifuge Tests." *Journal of Geotechnical and Geoenvironmental Engineering* 139(10): 1690-1698. https://doi.org/10.1061/(ASCE)GT.1943-5606.0000908

[20] Roy, J., Kumar, A., and Choudhury, D. (2018). "Natural Frequencies of Piled Raft Foundation including Superstructure Effect." *Soil Dynamics and Earthquake Engineering* 112: 69-75. https://doi.org/10.1016/j.soildyn.2018.04.048

[21] Sahraein, S. M. S., Takemura, J., and Seki, S. (2018). "An Investigation about Seismic Behavior of Piled Raft Foundation for Oil Storage Tanks using Centrifuge Modelling." *Soil Dynamics and Earthquake Engineering* 104: 210-227. https://doi.org/10.1016/j.soildyn.2017.10.010

[22] Sawant, V.A., and Ladhane, K. B. (2016). "Nonlinear FEA of Pile Group Subjected to Lateral Load." *Open Journal of Civil Engineering* 6: 19-30. https://doi.org/10.4236/ojce.2016.61003

[23] Ta, L. D. and Small, J. C. (1996). "Analysis of Piled Raft Systems in Layered Soils." *International Journal for Numerical and Analytical Methods in Geomechanics* 20: 57-72. https://doi.org/10.1002/(SICI)1096-9853(199601)20:1<57::AID-NAG807>3.0.CO;2-0

[24] Teji, B. T. and Ashango, A. A. (2023). "Performance Optimization of Piled Raft Foundations in Layered Soil under Uniform Vertical Loading using PLAXIS3D." Advances in Material Sciences and Engineering 2023: 1-11. https://doi.org/10.1155/2023/6693876

[25] Yamashita, K., Yamada, T., and Hamada, J. (2011). "Investigation of Settlement and Load Sharing on Piled Rafts by Monitoring Full-Scale Structures." *Soils and Foundations* 51(3): 513-532. https://doi.org/10.3208/sandf.51.513

[26] Yamashita, K., Hamada, J., Onimaru, S., and Higashino, M. (2012). "Seismic Behavior of Piled Raft with Ground Improvement Supporting a Base-Isolated Building on Soft Ground in Tokyo." *Soils and Foundations* 52(5): 1000-1015. https://doi.org/10.1016/j.sandf.2012.11.017

[27] Yamashita, K., Hamada, J., and Tanikawa, T. (2016). "Static and Seismic Performance of a Friction Piled Raft Combined with Grid-Form Deep Mixing Walls in Soft Ground." *Soils and Foundations* 56(3): 559-573. https://doi.org/10.1016/j.sandf.2016.04.020

[28] Zhang, L., Goh, S. H., and Liu, H. (2017). "Seismic Response of Pile-Raft-Clay System Subjected to a Long-Duration Earthquake: Centrifuge Test and Finite Element Analysis." *Soil Dynamics and Earthquake Engineering* 92: 488-502. https://doi.org/10.1016/j.soildyn.2016.10.018